

International Journal of Modern Physics: Conference Series
 © The Authors

White Dwarf Stars

S. O. Kepler, Alejandra Daniela Romero, Ingrid Pelisoli & Gustavo Ourique

*Departamento de Astronomia, Instituto de Física,
 Universidade Federal do Rio Grande do Sul,
 91501-970 Porto Alegre, RS, Brazil
 kepler@if.ufrgs.br*

Received 3 Feb 2017

White dwarf stars are the final stage of most stars, born single or in multiple systems. We discuss the identification, magnetic fields, and mass distribution for white dwarfs detected from spectra obtained by the Sloan Digital Sky Survey up to Data Release 13 in 2016, which lead to the increase in the number of spectroscopically identified white dwarf stars from 5 000 to 39 000. This number includes only white dwarf stars with $\log g \geq 6.5$ stars, i.e., excluding the Extremely Low Mass white dwarfs, which are necessarily the byproduct of stellar interaction.

Keywords: white dwarf; magnetic field; pulsar.

PACS numbers:

1. Introduction

White dwarf stars are the final evolutionary state of stars with initial masses up to $8.5\text{--}10.6 M_{\odot}^1$, corresponding to 95 – 97 % of all stars. The fraction depends on the stellar metallicity, which affects both the Initial-Mass-Function and the Initial-to-Final-Mass Relation. For single stars, the minimum mass of a present day white dwarf is around $0.30\text{--}0.45 M_{\odot}^2$, because progenitors that would become lower mass white dwarfs have main sequence evolution time larger than the age of the Universe. Such masses correspond, considering the mass-radius relation of white dwarfs, to a minimal $\log g \simeq 6.5$. Evolutionary models e.g. by Ref. 3 indicate that the maximum surface gravity for main sequence A stars, which have similar optical spectra to DA white dwarfs, corresponds to $\log g \leq 4.75$, even for very low metallicity. There is therefore a gap between low mass white dwarfs and main sequence stars, $4.75 \leq \log g \leq 6.5$.

Most white dwarfs do not generate energy from nuclear fusion, but radiate due to residual gravitational contraction. Because of the degenerate equation of state, contraction is accompanied by a loss of thermal energy instead of increase as in

This is an Open Access article published by World Scientific Publishing Company. It is distributed under the terms of the Creative Commons Attribution 3.0 (CC-BY) License. Further distribution of this work is permitted, provided the original work is properly cited.

the case of ideal gases; the evolution of white dwarfs is therefore often simply described as cooling. The radius of an average white dwarf star is of the same order of the Earth’s radius, which implies that they have small surface area, resulting in very large cooling times; it takes approximately 10^{10} years for the effective temperature of a normal mass white dwarf to decrease from 100 000 K to near 5 000 K. Consequently, the cool normal mass ones are still visible and among the oldest objects in the Galaxy⁴. Therefore, studying white dwarfs is extremely important to comprehend the processes of stellar formation and evolution in the Milky Way^{5,6}.

The progenitors of white dwarfs lose most of their envelope in the giant phases, where mass loss depends on metallicity. If the remainder H mass were above $\simeq 10^{-4}M_*$, or the He mass above $\simeq 10^{-2}M_*$ there would be observable nuclear burning in the white dwarf phase. The limits depend on the mass of the white dwarf. As shown in Table 1, most white dwarfs have atmospheres dominated by H, and the remainder by He. All other elements are only small traces, much less abundant than in the Sun, due to separation in the strong gravitational field⁷. The lightest elements float to the surface once the white dwarf cools below effective temperature $T_{\text{eff}} \simeq 100\,000$ K. Except for the H or He composition, the atmosphere of the white dwarfs in their later cooling evolution has thus lost all memory of the previous evolutionary phases.

We selected candidates to white dwarf stars from the 4.5 million SDSS spectra through their colors, automated spectra fitting by the SDSS pipeline, and targeted search of template spectra. After complete, consistent human identifications of each candidate white dwarf spectrum, we fitted the optical spectra to local thermodynamic equilibrium (LTE) grids of synthetic non-magnetic spectra derived from model atmospheres⁸. Our more recent DA model grid uses the $ML2/\alpha = 0.8$ convection approximation, and for the DBs we use the $ML2/\alpha = 1.25$ approximation. The DA grid extends up to $T_{\text{eff}} = 100\,000$ K, but NLTE effects are not included. Ref. 9 concluded pure hydrogen atmospheres of DA white dwarfs are well represented by LTE calculations for effective temperatures up to 80 000 K, but when traces of helium are present, non-local thermodynamic equilibrium (NLTE) effects on the Balmer lines occur, down to effective temperatures of 40 000 K. Ref. 9 concluded LTE models should exclude traces of helium for the consistent analysis of hydrogen dominated white dwarf spectra. We fitted the spectral lines and photometry separately⁸, selecting between the hot and cool solutions using photometry as an indicator. We include corrections to T_{eff} and $\log g$ based on three-dimensional convection calculations from Ref. 10.

At the cool end of our sample, $\log g = 6.5$ corresponds to a mass around $0.2 M_{\odot}$, well below the single mass evolution in the lifetime of the Universe. The He-core white dwarf stars in the mass range $0.2 - 0.45 M_{\odot}$, referred to as low-mass white dwarfs, are usually found in close binaries, often double degenerate systems¹¹, being most likely a product of interacting binary star evolution. More than 70% of those studied by Ref. 12 with masses below $0.45 M_{\odot}$ and all but a few with masses below $0.3 M_{\odot}$ show velocity variations^{13,14}. Ref. 2 suggests single low-mass white

dwarfs result from the evolution of old metal-rich stars that truncate evolution before the helium flash due to severe mass loss. They also conclude all white dwarfs with masses below $\simeq 0.3 M_{\odot}$ must be a product of binary star evolution involving interaction between the components, otherwise the lifetime of the progenitor on the main sequence would be larger than the age of the Universe.

2. Spectral fits

In Fig. 1 we show the results of our effective temperature and surface gravity determinations for all candidates. We calculated the single star evolutionary models shown in the figure with the MESA¹⁵ evolutionary code, including diffusion. In Fig. 2 the evolutionary models are those with rotation and diffusion of Ref. 16.

3. Spectral Classification

We looked for the following features to aid in the classification for each specified white dwarf subtype:

- Balmer lines — normally broad and with a steep Balmer decrement [DA but also DAB, DBA, DZA, and subdwarfs]
- HeI 4 471Å [DB, subdwarfs]
- HeII 4 686Å [DO, PG1159, sdO]
- C2 Swan band or atomic CI lines [DQ]
- CaII H & K [DZ, DAZ, DBZ]
- CII 4 367Å [HotDQ]
- Zeeman splitting [magnetic white dwarfs]
- featureless spectrum with significant proper motion [DC]
- flux increasing in the red [binary, most probably M companion]
- OI 6 158Å [Dox]

Table 1 shows the spectral classification for the 32 840 stars we identified as white dwarf stars from SDSS spectra. 84% are hydrogen atmosphere DAs.

Table 1. Spectral Classification

Stars	Spectra	Classification
27661	29262	DAs
2252	2403	DBs
722	778	DAH
1435	1494	DC
935	964	DZ
410	440	DQ
127	133	DO
19	21	DBH
1	1	Dox

4 *Kepler et al.*

3.1. $D\alpha\alpha$

Theoretically, stars with initial masses $7 M_{\odot} \leq M \leq 10.6 M_{\odot}$ will reach sufficiently high core temperatures, $T = 8\text{--}12 \times 10^8$ K — corresponding to center-of-mass energies from 1 to 3 MeV — to proceed to carbon burning, and produce either oxygen-neon (ONe) core white dwarfs, or undergo a core-collapse supernova (SNII) via electron capture on the products of carbon burning^{17,18,19,1}. The exact outcome

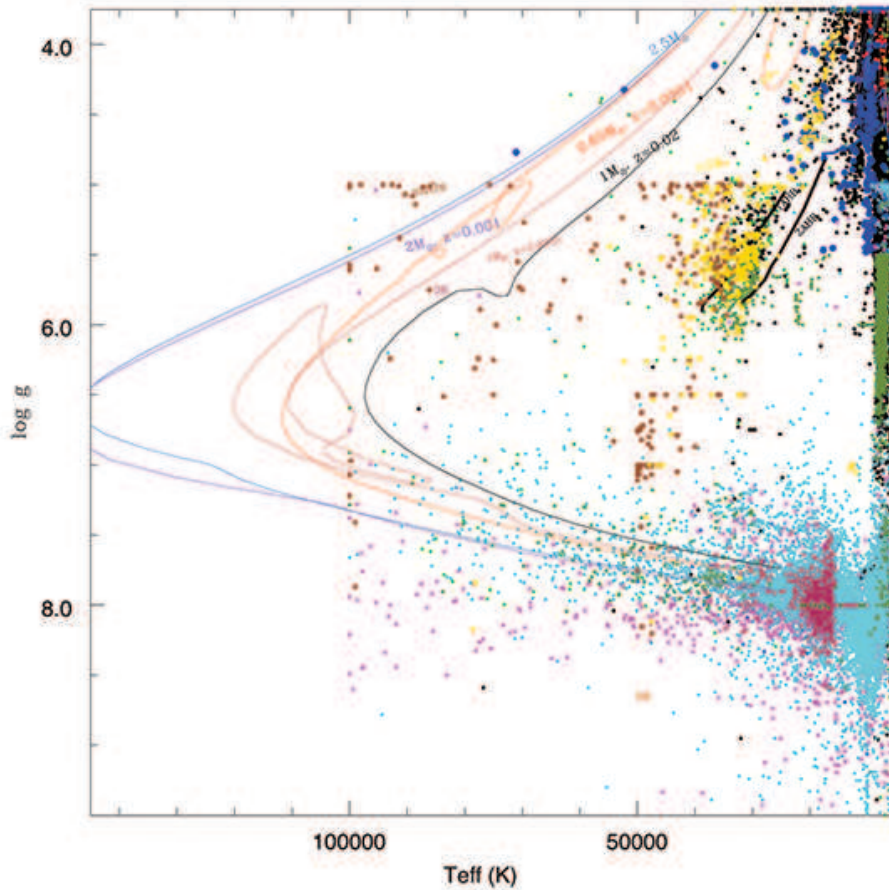


Fig. 1. Estimated effective temperature and superficial gravity for 79 440 blue stars in the Sloan Digital Sky Survey up to Data Release 13, and single star evolutionary models for different metallicities, showing there is a region in the middle of the diagram that no single star evolutionary models cover. Data of different colors represent distinct spectral classification and catalogs, DAs in light green, DBs in red, sdBs and sdOs in yellow, sdAs in dark green and black. The Zero Age Horizontal Branch (ZAHB) and Terminal Age Horizontal Branch (TAHB) plotted were calculated with solar composition models.

of stellar evolution in this mass range depends critically on the detailed understanding of the nuclear reaction rates involved, mass-loss, on the efficiency of convective mixing in the stellar cores²¹, and metallicity³. Ref. 22 found a white dwarf with oxygen dominated atmosphere, with no traces of hydrogen, helium or carbon, and with a mass of only $0.56 \pm 0.09 M_{\odot}$, not expected from evolutionary models, as such high-mass main sequence stars should result in massive ($M > 1 M_{\odot}$) white dwarfs²⁰.

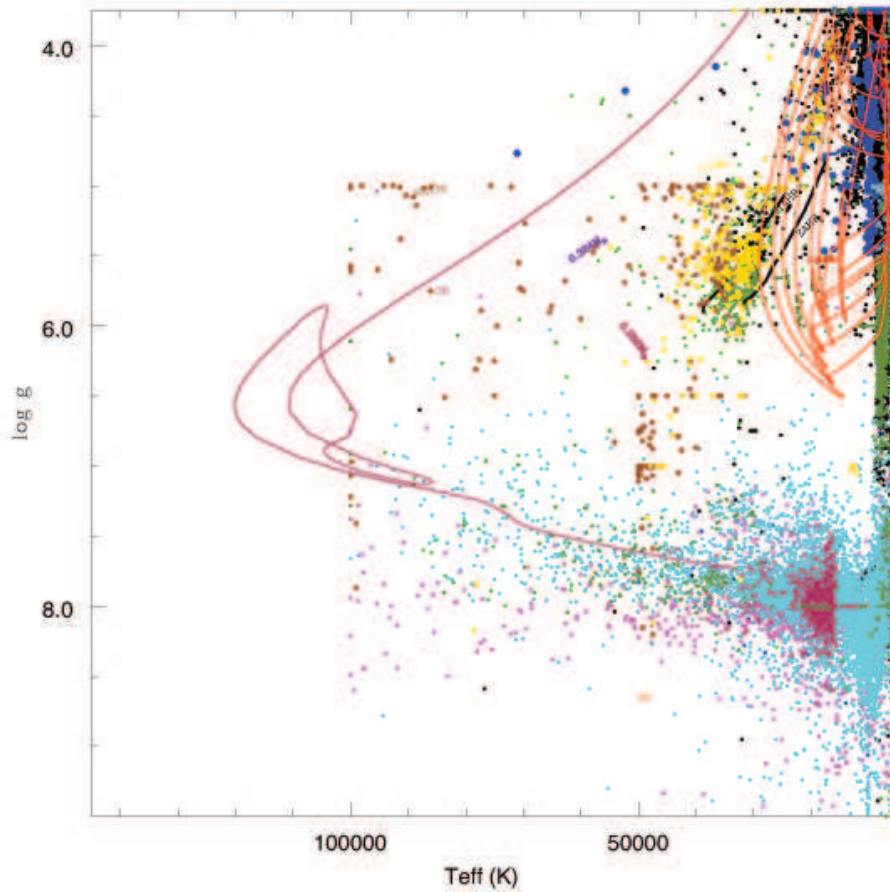


Fig. 2. Estimated effective temperature and superficial gravity for 79 440 blue stars in SDSS Data Release 13, and interacting binary star evolutionary models¹⁶, showing the region in the middle of the diagram is covered by interacting binary models.

6 *Kepler et al.*

3.2. *DZs*

Of the white dwarfs in our sample, 3% have spectra with metal lines, probably due to accretion of rocky material surrounding the stars^{23–26}. Calcium and magnesium in general have the strongest lines for white dwarfs at these temperatures. DZs were the first objects to show asteroidal material exists around stars and Ref. 27, 28 show multiple bodies are falling on one white dwarf.

3.3. *Extremely Low Mass white dwarfs*

DA white dwarf stars with masses $M \leq 0.45 M_{\odot}$ and $T_{\text{eff}} < 20\,000$ K are Low Mass and Extremely Low Mass (ELM) as found by Refs. 29, 12, 30, 13, 14, 31 and 32. Refs. 33 – 37 found pulsations in eight of these ELMs, similar to the pulsations seen in DAVs (ZZ Ceti stars), as described in Ref. 38. Ref. 39 found 17 pre-ELMs, i.e., helium-core white dwarf precursors, and Ref. 40, 41 report pulsations in six of them. Pulsations are an important tool to study the stellar interior, and Refs. 42 – 48 report on theoretical models and pulsations of ELMs. Refs. 49 and 50 show there are thousands of stars, photometrically classified as blue horizontal branch stars by Ref. 51, 52, 53, that have spectroscopic estimated surface gravities much higher than main sequence stars ($\log g \geq 4.75$) and therefore must have radii smaller than the Sun, classifying them as sdAs, in line with the hot subdwarfs reviewed by Ref. 54. Ref. 55 discuss they are possibly Extremely Low Mass white dwarf stars. Refs. 49, 56 show that photometrically selected white dwarfs have a contamination around 40%. Even the ones selected also from proper motion by Ref. 57 show significant contamination by non-white dwarf objects, when spectra are available.

Most stars that produced white dwarfs are born in binaries or multiple systems. Ref. 58 demonstrates that while around 70% of stars more massive than the Sun are in binaries, two-thirds of the most common stars, M type dwarf stars, are single. More than 10% of the spectroscopically identified white dwarfs in SDSS have red companions^{49,59}. Refs. 60, 61 show that nearly 25% of all main sequence binaries are close enough that mass transfer interactions occur when the more massive star becomes a red giant or an asymptotic giant star. If mass transfer exceeds the Eddington limit, the secondary star is not able to accrete the transferred material and the system evolves through a common envelope phase, i.e., the core of the giant and the main sequence companion orbit within the outer layers of the giant star, leading to the shrinkage of the orbit and the release of orbital energy. The orbital energy deposited into the envelope eventually ejects it. Therefore a close binary is formed by the core of the giant star and a main sequence companion, later a close white dwarf-main sequence binary. An ELM will be formed if the envelope is ejected before the helium-flash, which would happen if the star has initial mass too low, i.e., $M \lesssim 2M_{\odot}$, to reach conditions to fuse helium in the core before it becomes degenerate.

Systems in which a white dwarf is receiving mass from a nearby low mass star are classified as Cataclysmic Variables⁶². Accretion of mass by a white dwarf, or

the merger of two white dwarfs, may lead to a supernova (SNIa) explosion, if the system grows over the Chandrasekhar mass limit. The binary white dwarf system SDSS J065133.338+284423.37, with a 12.75 m orbital period, has been identified by Ref. 63, showing clear rapid orbital decay consistent with general relativity prediction due to gravitational wave radiation. White dwarfs have been identified as companions to millisecond pulsars^{64–76}.

Ref. 77 uses the Gaia parallaxes for 6 directly observed and 46 white dwarf stars in binary system to estimate their mass-radius relation. By Gaia second data release, in September 2017, the distance to thousand of white dwarf stars should be known, allowing a precise determination of the mass-radius relation for white dwarfs and clarifying the nature of the Extremely Low Mass white dwarfs and subdwarfs.

4. Mass Distribution

We estimated the masses of all DA white dwarfs found by Ref. 78, 79 and 49. There were no new optical stellar spectra in SDSS Data Release 13. For the DA mass distribution, we only consider spectra with $S/N \geq 15$ to have reliable mass determinations. We use the mass–radius relations of Refs. 80, 81 and 3 to calculate the mass of our stars from the T_{eff} and $\log g$ values obtained from our fits, after

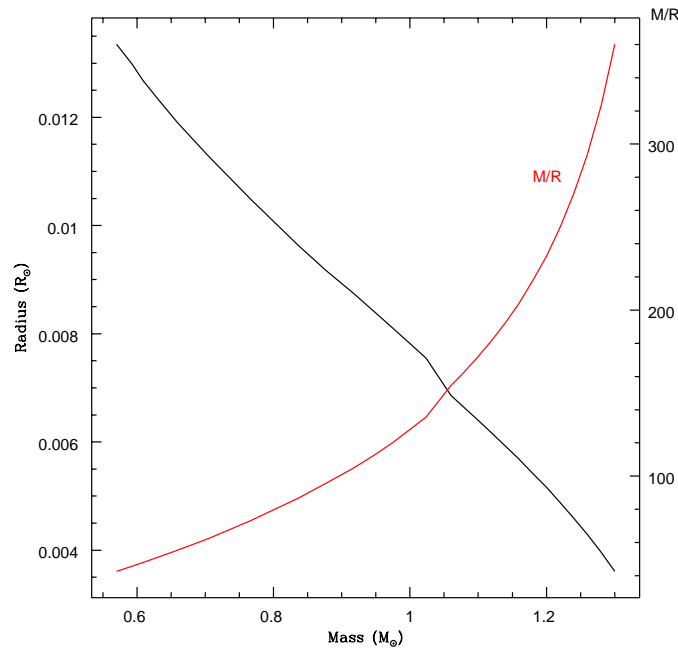


Fig. 3. Mass and radius of white dwarfs, calculated from C/O e O/Ne evolutionary models at $T_{\text{eff}} = 10\,000$ K.

8 *Kepler et al.*

correcting to 3D convection following Ref. 82.

Figure 4 shows the mass distribution by number for DAs with $T_{\text{eff}} \geq 13\,000$ K, where convection is unimportant, and for DBs with $T_{\text{eff}} \geq 16\,000$ K reported by Ref. 83. Because our surface gravities show an unexplained decrease below $T_{\text{eff}} = 10\,000$ K, Figure 5 shows the mass distribution for different cutoff temperatures.

Considering white dwarfs with larger mass have smaller radius, and therefore can only be seen to smaller distances in a magnitude limited survey as SDSS, we calculated the density by correcting the visible volume with the $1/V_{\text{max}}$ method of Ref. 84, up to a maximum $g=19$ magnitude, shown in Figure 5. The distribution shows that the DA and DB distributions have very different shapes. The DA's has a tail to larger masses, while the DB's is extended to lower masses. This is probably reflecting some limitation in the progenitors that can undergo very-late thermal pulses and become DBs.

5. Magnetic Fields

Ref. 85 presents a review on magnetic fields in white dwarf stars. When examining each white dwarf candidate SDSS spectrum by eye, we found 822 stars with Zeeman splittings indicating magnetic fields above 2 MG — the limit where the line splitting

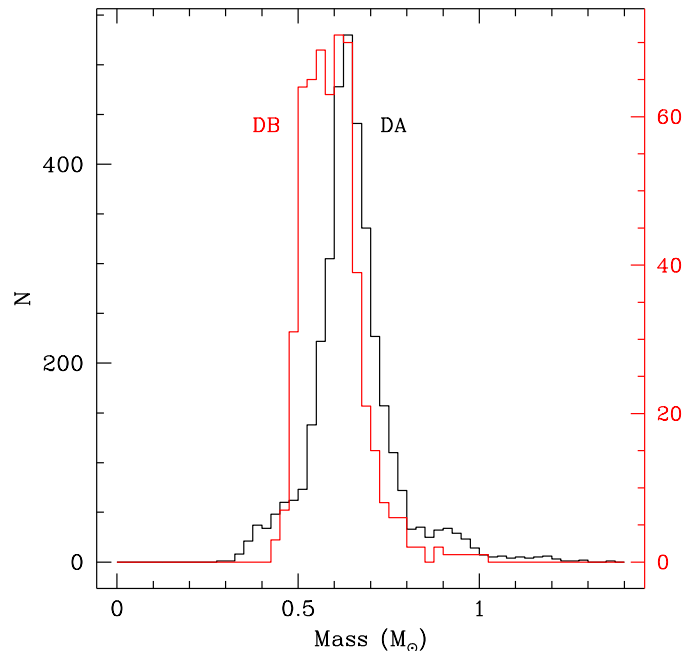


Fig. 4. Mass distribution by number for 3636 DAs with $T_{\text{eff}} \geq 13\,000$ K, $S/N_g \geq 15$ and $\langle S/N \rangle = 31$ in black and 549 DBs with $T_{\text{eff}} \geq 16\,000$ K, $S/N_g \geq 10$ and $\langle S/N \rangle = 21$ in red.

becomes too small to be identified at the SDSS spectral resolution⁸⁶.

If the line splitting and magnetic fields were not recognized, the spectral fittings of DA and DB models would have rendered too high $\log g$ determinations due to magnetic broadening being misinterpreted as pressure broadening. We estimated the mean fields for the new DAHs following Ref. 87 as being from 2 MG to 700 MG. We caution that stars with large fields are difficult to identify because fields above around 30 MG intermixes subcomponents between different hydrogen series components so much that, depending on effective temperature and signal-to-noise, it becomes difficult to identify the star as containing hydrogen at all, and affecting even the colors significantly. Additionally, white dwarf stars with fields above 100 MG (see Fig. 6) represent the intermediate regime in which the spectra have very few features, except for a few stationary transitions that have similar wavelengths for a reasonable distribution of magnetic fields over the surface of the star. We found significant Zeeman splittings in the spectra of around 4% of all white dwarfs. Both the low field limit and the high field limit are totally dominated by systematic effects, not the real limits. Polarization is hard to detect because it re-

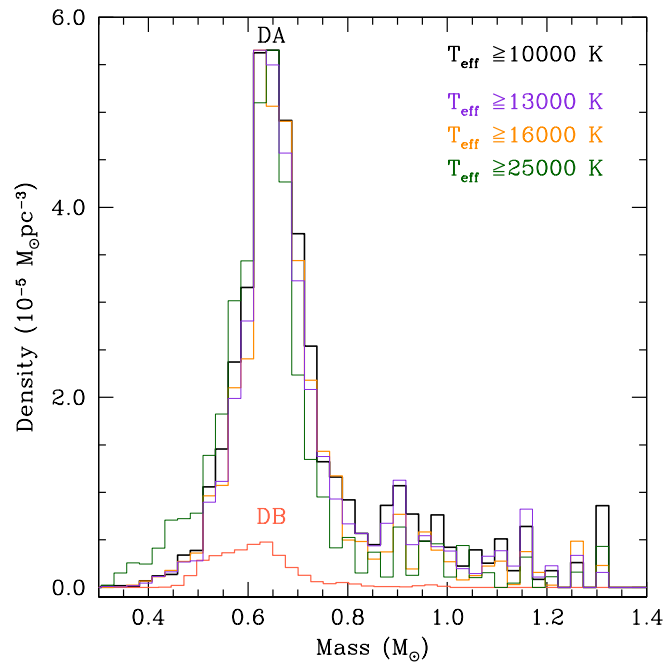


Fig. 5. Mass distribution corrected by the $1/V_{\max}$ method for DAs for different cutoff temperatures, and DB with $T_{\text{eff}} \geq 16000$ K. DAs with $T_{\text{eff}} \geq 10000$ K, $N=4054$, $\langle M \rangle = 0.647 \pm 0.002 M_{\odot}$ in black, $T_{\text{eff}} \geq 13000$ K, $N=3637$, $\langle M \rangle = 0.646 \pm 0.002 M_{\odot}$ in violet, $T_{\text{eff}} \geq 16000$ K, $N=3012$, $\langle M \rangle = 0.641 \pm 0.002 M_{\odot}$ in gold, $T_{\text{eff}} \geq 25000$ K, $N=1121$, $\langle M \rangle = 0.613 \pm 0.003 M_{\odot}$ in green.

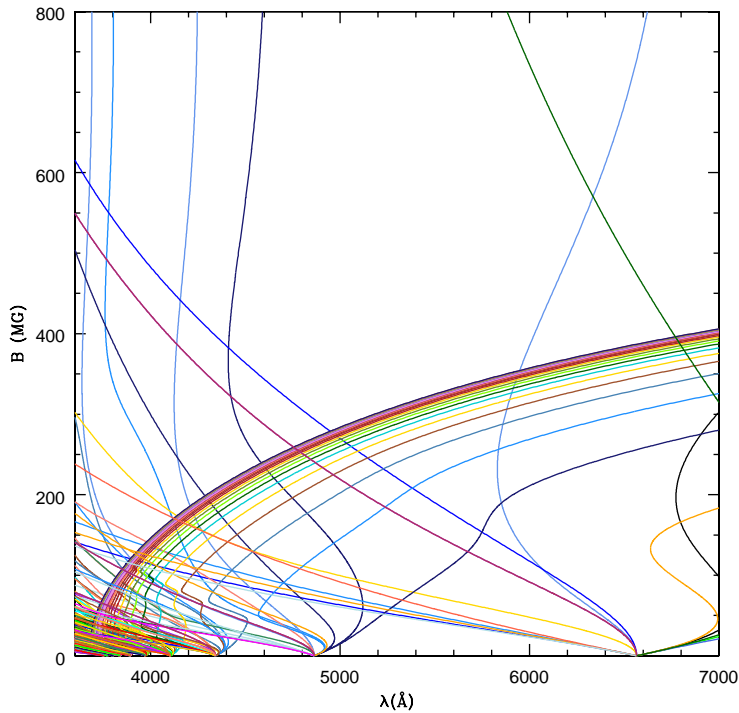


Fig. 6. Theoretical Zeeman splittings for hydrogen lines in a dipole magnetic field, showing that even fields around 1 MG produce large splittings of the higher Balmer lines^{109–111}.

quires signal-to-noise well above 100, as the fraction of polarized light is in general smaller than 1%. Polarimetric studies by Ref. 89–90 have shown fields larger than dozens of kilogauss for more than 10% of the white dwarfs. The most massive white dwarf stars have progenitors between O and B main sequence stars. Only one dozen of O-type stars have spectroscopically confirmed magnetic fields, from 50 to 400 G, while A and B stars have fields from 10 to 10^4 Gauss⁹¹. Even though convection do amplify the magnetic field, most fields are generated during the protostar phase.

The magnetic field detected changes as the star rotates, as in all bodies the rotation axis is not aligned with the magnetic field axis. SDSS J030407.40-002541.74, with $g=17.75$, was first classified as a magnetic white dwarf by Ref. 92, who estimated the magnetic field from one SDSS spectrum, with Plate-MJD-Fiber=411-51817-172. They noticed the $H\alpha$ Zeeman triplet split by 200 Å, and detected multiple Zeeman components of $H\beta$ and $H\gamma$. They fitted the spectrum with a $T_{\text{eff}} = 15\,000$ K white dwarf model, with a dipole field strength $B_d = 10.8$ MG and a magnetic inclination $i = 50^\circ$ (where $i = 90^\circ$ corresponds to an equator-on view). The model spectrum provided a good match for both the continuum slope and the strength of the Zeeman absorption lines. The most noticeable shortcoming of their fit was the

poor agreement in the $\sigma = -1$ component of $H\beta$. Ref. 93 estimated $T_{\text{eff}} = 11\,500$ K with a dipole field strength $B_d = 11$ MG and a magnetic inclination $i = 60^\circ$ from the same spectrum. Ref. 87 reanalyzed the same spectrum and fitted an offset dipole with $T_{\text{eff}} = 11\,500$ K, assuming $\log g = 8.00$, and obtained $B = 11.13 \pm 0.97$ MG, $z_{\text{off}} = 0.27 \pm 0.10 r_{\text{WD}}$, and an inclination angle of $i = 52 \pm 17$ deg. Ref. 86 estimated a varying magnetic field for the 6 SDSS spectra of the star (Table 2), assuming dipole magnetic distribution, obtaining $B \simeq 10\text{--}19$ MG from the $H\alpha$ and $H\beta$ splittings.

Table 2. SDSS spectra and individual spectrum magnetic field estimates.

Date Obs.	P-M-F	$B_{H\alpha}$ (MG)	$B_{H\beta}$ (MG)	$(S/N)_g$
2000-09-30 10:36:49 3 exp. 2700s	0411-51817-172	11	10	23
2000-11-25 05:47:22 3 exp. 2700s	0411-51873-172	19	18	22
2001-01-03 04:33:00 6 exp. 8151s	0411-51914-169	10	10	15
2001-10-21 10:24:01 3 exp. 3504s	0710-52203-311	11	11	21
2001-10-23 09:46:21 4 exp. 5408s	0709-52205-120	11	11	27
2005-01-08 02:55:09 5 exp. 6300s	2048-53378-280	10	10	26

A fit to the optical SDSS u,g,r colors with non-magnetic models results in $T_{\text{eff}} = 12\,200 \pm 300$ K, $\log g = 8.2 \pm 0.1$, and mass $M = 0.72 \pm 0.06 M_\odot$, all unreliable because the large Zeeman splittings affect the colors, specially u, substantially. A fit to the r,i,z colors results in $T_{\text{eff}} = 13\,500 \pm 500$ K, but the $\log g$ went to the high border of the grid. GALEX observations $\text{nuv} = 18.11 \pm 0.04$, $\text{fuv} = 18.62 \pm 0.07$ are consistent with $T_{\text{eff}} \simeq 12\,000$ K, but the spectra does not fit from the red to the blue (see Fig.7).

The Catalina Real-time Transient Survey has 311 measurements with a few measurements significantly brighter, with a mean of $V_{CSS} = 17.76 \pm 0.05$ and a change from 17.89 ± 0.11 to 17.18 ± 0.16 in 14 minutes. The timescale of change is of the order of a few hours, but there is no periodic variation found. The 32 SDSS photometric measurements also show variations in color.

5.1. Observations

To test for short timescale variations and obtain a higher signal-to-noise average spectrum, we obtained 3×1800 s exposures for SDSS J030407.40-002541.92 with the Soar 4.1 m telescope on the night of 2010-09-10 at 06:14:01.77 UT, with a 600 l/mm volume phase holographic grating and a GG-385 red blocking filter on the Goodman Spectrograph⁹⁴, reaching a $S/N \simeq 40$ in the continuum. Goodman is mounted at the SOAR Optical Nasmyth and its detector is a $4\text{k} \times 4\text{k}$ Fairchild 486 back-illuminated CCD, with a un-binned plate scale of 0.15 arcsec/pixel. The $\sigma = -1$ component of $H\beta$ was missing, just like Ref. 92 noticed for the Plate-MJD-Fiber=0411-51817-172 SDSS spectra obtained in 2000-09-30. We did not detect significant changes from spectrum to spectrum (06:14:01, 06:46:06, and 07:17:28 UT). Ref. 95 demonstrated isolated magnetic white dwarfs show photometric variability

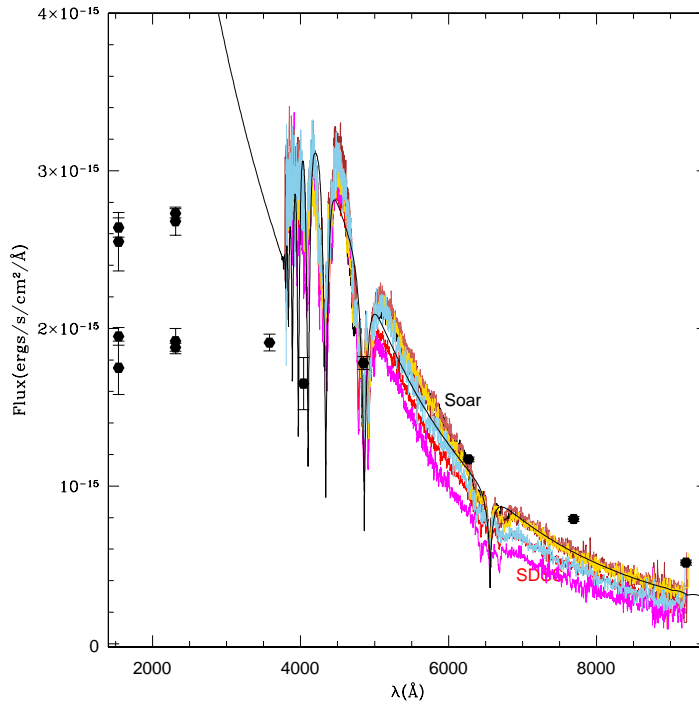


Fig. 7. Sloan Digital Sky Survey and SOAR spectra of the DAH star SDSS J030407.40-002541.92, showing the Zeeman splittings changes from spectrum to spectrum. The thin black line is a non-magnetic model with $T_{\text{eff}} = 11500$ K and $\log g = 8$, just to guide the eye. The photometric measurements are plotted at their central wavelengths. Due to their broad filters, they represent integrations over absorption lines. The depression in the GALEX colors FUV and NUV are not caused by absorption lines and are due to the magnetic field. Changes in magnitude are also seen in the optical.

on timescale from hours to several years, probably associated with rotation. Our spectra from SDSS and SOAR is too sparse to estimate the timescale of variability.

5.2. Analysis

The field structure over the surface of the white dwarf becomes accessible to measurement via the profiles of the photospheric Zeeman-broadened Balmer absorption lines, an approach dubbed Zeeman tomography⁹⁶. Refs. 97, 98 show the field geometries of two isolated white dwarfs, HE 1045–0908 and PG 1015+014, were significantly more complex than simple centered or offset dipoles. Ref. 99 applied the method to cataclysmic variables and Ref. 87 applied it to 150 magnetic white dwarf stars observed by SDSS.

The model spectra we fitted were calculated with a radiative transfer code for magnetized white dwarf atmospheres. For a given temperature and pressure struc-

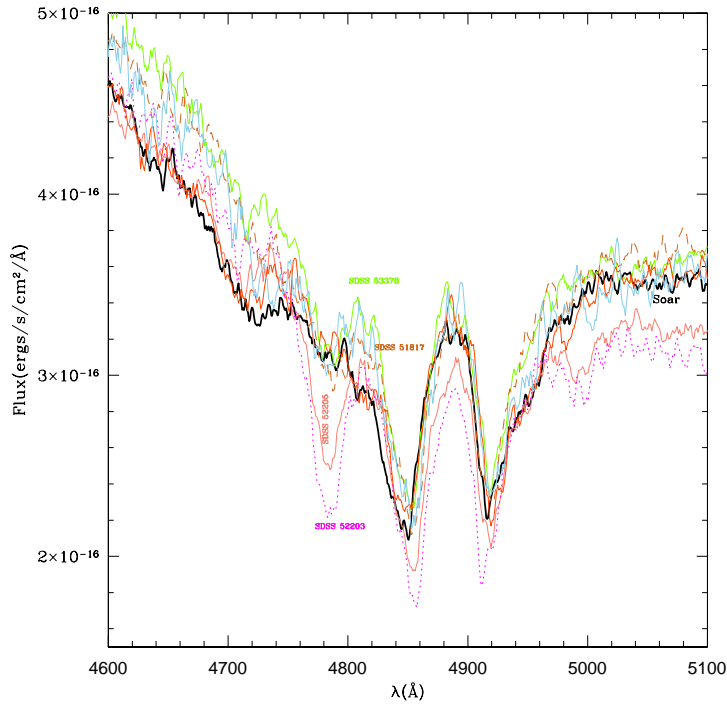


Fig. 8. Sloan Digital Sky Survey and SOAR spectra of the DAH star SDSS J030407.40-002541.92 around H β , showing the Zeeman splitting changes from a triplet to a doublet, at different epochs.

ture of a model atmosphere (T_{eff} , $\log g$) and a given magnetic field vector with respect to the line of sight and the normal on the surface of the star, it calculates theoretical flux and polarization spectra^{100,101}. The model spectra were calculated assuming a surface gravity of $\log g = 8$, considering DAs show a sharp peak in the mass distribution around this value^{103,104,10}, and we do not have a clear way to estimate the mass of the star. Considering no polarization information is available for this star, our analysis is limited to the flux spectra (Stokes parameter I). Limb darkening is accounted for by a simple linear scaling law⁹⁶. We determine the magnetic field geometry with the code described in Ref. 87. This code calculates the total flux (and circular polarization) spectra for an arbitrary magnetic field topology by adding up appropriately weighted model spectra for a large number of surface elements and then evaluating the goodness of fit. Magnetic field geometries are accounted for by multi-pole expansions of the scalar magnetic potential. The individual multi-pole components may be independently oriented with respect to the rotation axis of the white dwarf and offset with respect to its center, allowing in principle for rather complex surface field topologies. Additional free parameters are

the white dwarf effective temperature and the inclination of the rotation axis with respect to the line of sight. The observed spectra was fitted using an evolutionary algorithm¹⁰⁵ with a least-squares quality function. Additionally to the Zeeman effect, Stark broadening is considered. For the case when the electric and magnetic fields are parallel, Ref. 106 estimated the effect on stationary line components, which are transitions that vary slowly in wavelength for large intervals of magnetic field strengths. Stationary lines are more pronounced than non-stationary lines, as they are not smeared out extensively due to the variation of the magnetic field strength over the stellar surface. However, no atomic data for hydrogen in the presence of both a magnetic and electric field are available for arbitrary strengths and arbitrary angles between two fields. Therefore, only a crude approximation¹⁰⁰ is used in the model and systematic uncertainties are unavoidable, particularly in the low-field regime (≤ 5 MG) where the Stark effect dominates. Consequently, effective temperatures and surface gravities derived from fitting the Balmer lines alone are less reliable than in the case of non-magnetic white dwarfs. This may also result in disagreements with temperature estimates derived from the continuum slope. Time-resolved analysis for rotating single magnetic white dwarfs is instrumental in determining rather complex field structures [e.g. VLT observations^{96,97,98}]. However this usually relies on the preliminary knowledge of period which is usually derived via photometry, separately. Although the individual SDSS fiber spectra exists with 15 minute exposure time, due to the lack of information on spin period, we constrained ourselves to the co-added spectra which includes 3 to 6 individual spectra with total exposure time of at least 45 minutes (see Table 2). For white dwarfs, the dipole magnetic field Ohmic decay timescale is 10^{10} yr and even the higher multi-poles can live for such a long period of time¹⁰⁷.

Figures 9 and 10 shows two graphic forms to present the field distribution across the surface of the star: (i) the $B \times \cos \phi$ diagram that depict the frequency distribution of field vectors over the surface of the star corresponding to the spectrum; and (ii) a synthetic picture of the field distribution. The latter include (a) the field strength B , (b) $\cos = B_l/B$ with B_l the field component along the line of sight.

To extend the calculations of the splittings for hydrogen levels higher than $n=7$ for these fields, where perturbation theory is no longer applicable^{100,108}, Refs. 109, 110 extended the calculations to $n=11$. This was achieved by using a two-dimensional finite element expansion of the wave functions in terms of B -splines in the directions parallel and perpendicular to the magnetic field, instead of using asymptotically valid basis expansions in terms of spherical harmonics or Landau orbitals, as has been previously done in the literature, which fails either in the high-field or the low-field regime, respectively. In this way energies could be calculated for 300 states with an accuracy of better than 10^{-6} Rydberg across several symmetry subspaces over the entire regime of magnetic field strengths. The wealth of the resulting wavelength information is the basis for the analysis of the spectra presented in this paper. Details of the computational method can be found in Ref. 111, and results from 0 to 800 MG are shown in Fig. 6.

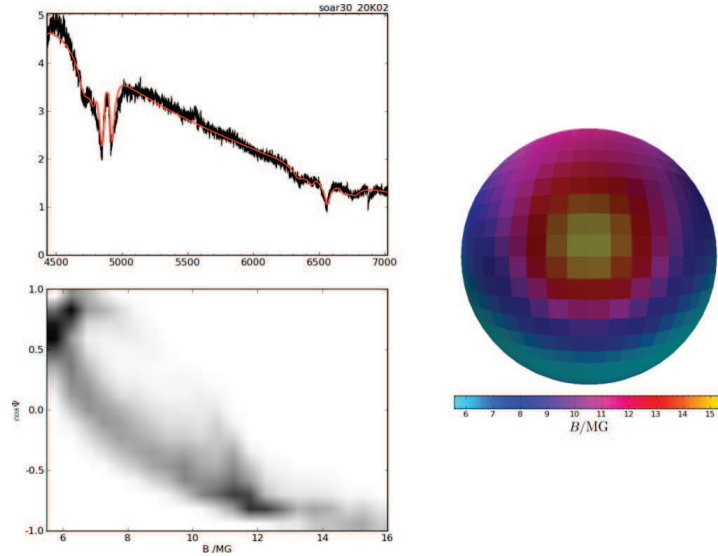


Fig. 9. Surface magnetic field distribution corresponding to the SOAR average spectrum, calculated by Baybars Külebi.

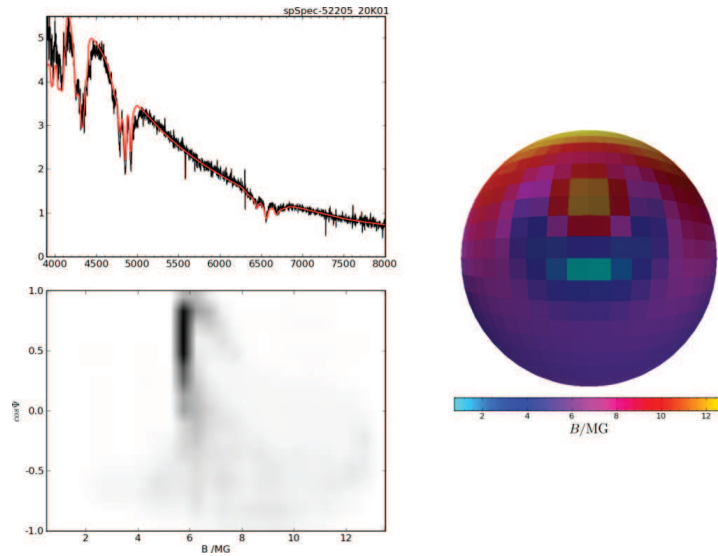


Fig. 10. Surface magnetic field distribution corresponding to the spectrum shown.

The combined effect of electric and magnetic fields on the spectral lines is very complicated and has been studied only for special cases of the geometry^{106,87}. Detailed model grids, which include also the effect of the magnetic field on the radiative transfer are not yet available.

We demonstrate the Zeeman splitting of the magnetic DA white dwarf SDSS J030407.40-002541.92 shows complex field distribution across the surface of the star, with a mean value of $B \simeq 13$ MG, and the Zeeman components change from different spectra, probably due to rotation of the star with the magnetic axis not aligned to the rotation axis.

Ref. 112 discuss how magnetic field can suppress convection in white dwarfs, resulting in magnetically generated spots on the stellar surface that can cause the observed variability, both spectral and photometric, when the star rotates. They also discuss that a magnetic field of the order of the observed in SDSS J030407.40-02541.74 can totally suppress convection, affecting the cooling of the white dwarf. The fast and irregular variations we see in SDSS J030407.40-02541.74 are different from the stable ones they report for the weaker magnetic field WD 1953-011.

6. Rotation

In general the measured rotation period for single white dwarfs ranges from 1 h to 18 d, with a median around 1 d¹¹³. The fastest single white dwarf rotator from asteroseismological measurements (Table 3) is the $0.79 M_{\odot}$ DAV SDSS J161218.08+083028.1 discovered by Ref. 115, assuming the two observed periods at 115.0 s and 117.0 s are two components of a rotation triplet.

There are two known binary systems with rotation periods around dozens of seconds, called white dwarf pulsars, AE Aquarii and AR Scorpii^{116,117}, in line with the models of Ref. 118.

For magnetic white dwarfs, the $P_{\text{rot}} = 725$ s fast rotator $1.34 M_{\odot}$ 450 MG DAH EUVE J0317-855 (1RXS J031713.9-853231) listed in Table 2 of Ref. 113 is in a double degenerate system with the $T_{\text{eff}} = 15600$ K white dwarf LB 9802¹¹⁴. Ref. 119 analyzed a non-interacting double white dwarf system NLTT 12758 of a fast spinning ($P_{\text{rot}} \simeq 23$ m) 3.1 MG $0.69 M_{\odot}$ white dwarf and a non-magnetic $0.83 M_{\odot}$ white dwarf in a 1.154 d orbit.

Differential rotation in white dwarfs was studied by Refs. 120 – 123, using the change in rotation splitting of non-radial pulsations, agreeing with the evidence of substantial loss of angular momentum on the red giant branch from asteroseismology of red giant stars^{124,125}.

7. Axions and Dark Mass

Axions are the best candidates for dark mass¹²⁶. Refs.127 – 132 show white dwarf pulsations and luminosity function are consistent with extra cooling caused by axions of masses around 17 ± 4 meV.

8. Population synthesis

We did a population synthesis analysis and computed a theoretical mass distribution through a Monte Carlo simulation — fitting single star initial mass functions, initial-to-final mass relations for masses $0.45 M_{\odot} \leq M < 1.0 M_{\odot}$ — to obtain a history of

Table 3. Rotation periods of white dwarfs as determined via asteroseismology.

Star	P_{rot} [h]	T_{eff}	Type	M [M_{\odot}]
RX J2117.1+3412	28	170000	GW Vir	0.72
PG 1159-035	33	140000	GW Vir	0.54
NGC 1501	28	134000	[WCE]	0.56
PG 2131+066	5	95000	GW Vir	0.55
PG 1707+427	16	85000	GW Vir	0.53
PG 0122+200	37	80000	GW Vir	0.53
PG 0112+104	10.17	31040	DBV	0.58
KIC 8626021	43	29700	DBV	0.56
EC 20058-5234	2	25500	DBV	0.65
GD 358	29	23740	DBV	0.54
G 226-29	9	12510	ZZ Ceti	0.83
G 185-32	15	12470	ZZ Ceti	0.67
SDSS J113655.17+040952.6	2.6	12330	ZZ Ceti	0.55
SDSS J161218.08+083028.1	0.93	12330	ZZ Ceti	0.79
Ross 548	37	12300	ZZ Ceti	0.63
GD 165	50	12220	ZZ Ceti	0.68
LP 133-144	41.8	12150	ZZ Ceti	0.59
KIC 11911480	86.4	12160	ZZ Ceti	0.58
L 19-2	13	12070	ZZ Ceti	0.69
HS 0507+0435	41	12010	ZZ Ceti	0.73
EC 14012-1446	14.4	12020	ZZ Ceti	0.72
KUV 11370+4222	5.56	11940	ZZ Ceti	0.72
G 29-38	32	11910	ZZ Ceti	0.72
HL Tau 76	53	11470	ZZ Ceti	0.55
SDSS J171113.01+654158.3	16.4	11130	ZZ Ceti	0.90
GD 154	50.4	11120	ZZ Ceti	0.65
KIC 4552982	15.0	10860	ZZ Ceti	0.71
SDSS J094000.27+005207.1	11.8	10590	ZZ Ceti	0.82

The effective temperatures and masses are corrected to 3D convection¹⁰.

star formation for the DAs. With our calculated lifetimes from ZAMS to the present cooling stage, all white dwarfs born 12 Gyr ago are below $T_{\text{eff}} \simeq 10\,000\text{K}$, most are expected to be around 4500 K. For our sample with $T_{\text{eff}} \geq 13\,000\text{K}$, Figure 11 shows the mean mass around $0.64 M_{\odot}$ requires a burst of star formation in the last 2 Gyr, as a white dwarf with such mass has a short lived progenitor mass with a mass around $2.5 M_{\odot}$. This is in contrast with the uniform star formation estimated by Ref. 133 from the $ML2/\alpha = 0.6$ mass distribution of Ref. 103. These results indicate most white dwarfs are cooler than our present sample and we must develop ways to disentangle them from red dwarfs. Such cool helium atmosphere white dwarfs show no lines in the spectra, while hydrogen atmosphere ones show only a weak H α line. Proper motions and parallaxes are therefore the key separators, as cool white dwarfs are much fainter than red dwarfs at similar temperatures. Therefore GAIA will be crucial for their identification.

Acknowledgments

SOK, ADR, GO and IP are supported by CNPq-Brazil. This research has made use of NASA's Astrophysics Data System and of the cross-match service provided by CDS, Strasbourg. Funding for the Sloan Digital Sky Survey has been provided by the Alfred P. Sloan Foundation, the U.S. Department of Energy Office of Science, and the Participating Institutions. The SDSS web site is www.sdss.org. Based on observations obtained at the Southern Astrophysical Research (SOAR) telescope, which is a joint project of the Ministério da Ciência, Tecnologia, e Inovação (MCTI) da República Federativa do Brasil, the U.S. National Optical Astronomy Observatory (NOAO), the University of North Carolina at Chapel Hill (UNC), and Michigan State University (MSU).

9. References

References

1. Woosley, S. E., & Heger, A. 2015, *Astrophysical Journal*, 810, 34
2. Kilic, M., Stanek, K. Z., & Pinsonneault, M. H. 2007, *Astrophysical Journal*, 671,

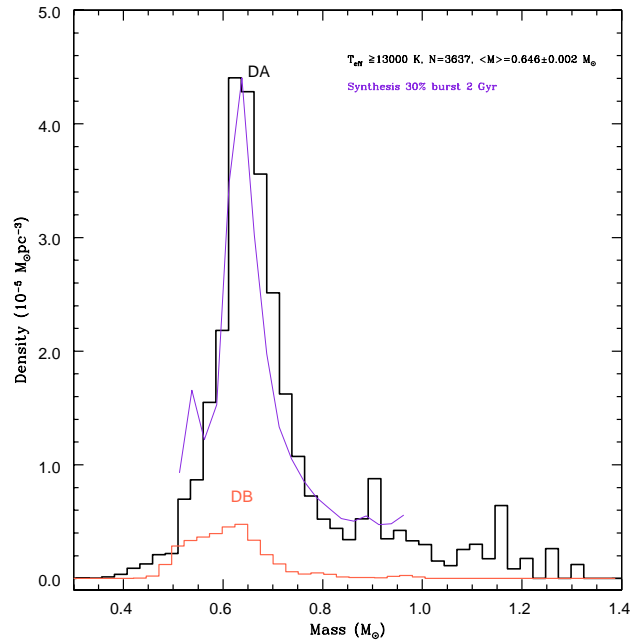


Fig. 11. Mass distribution corrected by the $1/V_{\text{max}}$ method for the 3637 DAs with $T_{\text{eff}} \geq 13000 \text{ K}$, $\langle M \rangle = 0.646 \pm 0.002 M_{\odot}$, and DBs with $T_{\text{eff}} \geq 16000 \text{ K}$. The blue line shows a population synthesis with a 30% burst 2 Gyr ago, to account for the high mean mass. The theoretical mass distribution represented by the population synthesis does not include either He-core or O-Ne-core models.

761

3. Romero, A. D., Campos, F., & Kepler, S. O. 2015, *Monthly Notices of the Royal Astronomical Society*, 450, 3708
4. García-Berro, E., & Oswalt, T. D. 2016, *New Astronomy Reviews*, 72, 1
5. Winget, D. E., Hansen, C. J., Liebert, J., et al. 1987, *Astrophysical Journal Letters*, 315, L77
6. Campos, F., Bergeron, P., Romero, A. D., et al. 2016, *Monthly Notices of the Royal Astronomical Society*, 456, 3729
7. Schatzman, E. 1948, *Nature*, 161, 61
8. Koester, D. 2010, *Memorie della Societa Astronomica Italiana*, 81, 921
9. Napiwotzki, R. 1997, *Astronomy & Astrophysics*, 322, 256
10. Tremblay, P.-E., Ludwig, H.-G., Steffen, M., & Freytag, B. 2013, *Astronomy & Astrophysics*, 552, A13
11. Marsh, T. R., Dhillon, V. S., & Duck, S. R. 1995, *Monthly Notices of the Royal Astronomical Society*, 275, 828
12. Kilic, M., Brown, W. R., Allende Prieto, C., et al. 2011, *Astrophysical Journal*, 727, 3
13. Brown W. R., Kilic M., Allende Prieto C., Gianninas A., Kenyon S. J., 2013, *Astrophysical Journal*, 769, 66
14. Gianninas, A., Hermes, J. J., Brown, W. R., et al. 2014, *Astrophysical Journal*, 781, 104
15. Paxton, B., Marchant, P., Schwab, J., et al. 2015, *Astrophysical Journal Supplement Series*, 220, 15
16. Istrate, A. G., Marchant, P., Tauris, T. M., et al. 2016, *Astronomy & Astrophysics*, 595, A35
17. García-Berro, E., & Iben, I. 1994, *Astrophysical Journal*, 434, 306
18. Doherty C. L., Gil-Pons P., Siess L., Lattanzio J. C., Lau H. H. B., 2015, *Monthly Notices of the Royal Astronomical Society*, 446, 2599.
19. Nomoto, K. 2014, *IAU Symposium Supernova Environmental Impacts*, 296, 27
20. Cummings, J. D., Kalirai, J. S., Tremblay, P.-E., Ramirez-Ruiz, E., & Bergeron, P. 2016, *Astrophysical Journal Letters*, 820, L18
21. Straniero, O., Domínguez, I., Imbriani, G., & Piersanti, L. 2003, *Astrophysical Journal*, 583, 878
22. Kepler, S. O., Koester, D., & Ourique, G. 2016, *Science*, 352, 67
23. Graham J. R., Matthews K., Neugebauer G., Soifer B. T., 1990, *Astrophysical Journal*, 357, 216
24. Jura M., 2003, *Astrophysical Journal*, 584, L91
25. Koester D., Gänsicke B. T., Farihi J., 2014, *Astronomy & Astrophysics*, 566, A34
26. Farihi, J. 2016, *New Astronomy Reviews*, 71, 9
27. Vanderburg, A., Johnson, J. A., Rappaport, S., et al. 2015, *Nature*, 526, 546
28. Gänsicke, B. T., Aungwerojwit, A., Marsh, T. R., et al. 2016, *Astrophysical Journal Letters*, 818, L7
29. Brown, W. R., Kilic, M., Allende Prieto, C., & Kenyon, S. J. 2010, *Astrophysical Journal*, 723, 1072
30. Brown W. R., Kilic M., Allende Prieto C., Kenyon S. J., 2012, *Astrophysical Journal*, 744, 142
31. Gianninas, A., Kilic, M., Brown, W. R., Canton, P., & Kenyon, S. J. 2015, *Astrophysical Journal*, 812, 167
32. Brown, W. R., Gianninas, A., Kilic, M., Kenyon, S. J., & Allende Prieto, C. 2016, *Astrophysical Journal*, 818, 155

33. Hermes, J. J., Montgomery, M. H., Winget, D. E., et al. 2012, *Astrophysical Journal Letters*, 750, L28
34. Hermes, J. J., Montgomery, M. H., Winget, D. E., et al. 2013, *Astrophysical Journal*, 765, 102
35. Hermes, J. J., Montgomery, M. H., Gianninas, A., et al. 2013, *Monthly Notices of the Royal Astronomical Society*, 436, 3573
36. Bell, K. J., Kepler, S. O., Montgomery, M. H., et al. 2015, 19th European Workshop on White Dwarfs, 493, 217
37. Bell, K. J., Gianninas, A., Hermes, J. J., et al. 2016, arXiv:1612.06390
38. Van Grootel, V., Fontaine, G., Brassard, P., & Dupret, M.-A. 2013, *Astrophysical Journal*, 762, 57
39. Maxted, P. F. L., Bloemen, S., Heber, U., et al. 2014, *Monthly Notices of the Royal Astronomical Society*, 437, 1681
40. Maxted, P. F. L., Serenelli, A. M., Marsh, T. R., et al. 2014, *Monthly Notices of the Royal Astronomical Society*, 444, 208
41. Gianninas, A., Curd, B., Fontaine, G., Brown, W. R., & Kilic, M. 2016, *Astrophysical Journal Letters*, 822, L27
42. Córscico, A. H., & Althaus, L. G. 2014, *Astronomy & Astrophysics*, 569, A106
43. Córscico, A. H., & Althaus, L. G. 2014, *Astrophysical Journal Letters*, 793, L17
44. Istrate, A. G., Tauris, T. M., & Langer, N. 2014, *Astronomy & Astrophysics*, 571, A45
45. Istrate, A. G., Tauris, T. M., Langer, N., & Antoniadis, J. 2014, *Astronomy & Astrophysics*, 571, L3
46. Córscico, A. H., & Althaus, L. G. 2015, 19th European Workshop on White Dwarfs, 493, 221
47. Córscico, A. H., Althaus, L. G., Calcaferro, L. M., et al. 2016, arXiv:1609.01352
48. Istrate, A. G., Fontaine, G., Gianninas, A., et al. 2016, *Astronomy & Astrophysics*, 595, L12
49. Kepler, S. O., Pelisoli, I., Koester, D., et al. 2016, *Monthly Notices of the Royal Astronomical Society*, 455, 3413
50. Kepler, S. O., Koester, D., Romero, A. D., Ourique, G., & Pelisoli, I. 2016, arXiv:1610.00371
51. Xue, X. X., Rix, H. W., Zhao, G., et al. 2008, *Astrophysical Journal*, 684, 1143-1158
52. Xue, X.-X., Rix, H.-W., Yanny, B., et al. 2011, *Astrophysical Journal*, 738, 79
53. Carollo, D., Beers, T. C., Placco, V. M., et al. 2016, *Nature Physics*, 12, 1170
54. Heber, U. 2016, *Publications of the Astronomical Society of the Pacific*, 128, 082001
55. Pelisoli, I., Kepler, S. O., Koester, D., & Romero, A. D. 2016, arXiv:1610.05550
56. Gentile Fusillo N. P., Gänsicke B. T., Greiss S., 2015, *Monthly Notices of the Royal Astronomical Society*, 448, 2260
57. Munn, J. A., Harris, H. C., von Hippel, T., et al. 2017, *Astronomical Journal*, 153, 10
58. Lada, C. J. 2006, *Astrophysical Journal Letters*, 640, L63
59. Rebassa-Mansergas, A., Ren, J. J., Parsons, S. G., et al. 2016, *Monthly Notices of the Royal Astronomical Society*, 458, 3808
60. Farihi, J., Hoard, D. W., & Wachter, S. 2010, *Astrophysical Journal Supplement Series*, 190, 275
61. Nebot Gómez-Morán, A., Gänsicke, B. T., Schreiber, M. R., et al. 2011, *Astronomy & Astrophysics*, 536, A43
62. Knigge, C., Baraffe, I., & Patterson, J. 2011, *Astrophysical Journal Supplement Series*, 194, 28

63. Hermes, J. J., Kilic, M., Brown, W. R., et al. 2012, *Astrophysical Journal Letters*, 757, L21
64. Durant, M., Kargaltsev, O., Pavlov, G. G., et al. 2012, *Astrophysical Journal*, 746, 6
65. Tauris, T. M., Langer, N., & Kramer, M. 2012, *Monthly Notices of the Royal Astronomical Society*, 425, 1601
66. Antoniadis, J. 2014, *Astrophysical Journal Letters*, 797, L24
67. Jia, K., & Li, X.-D. 2014, *Astrophysical Journal*, 791, 127
68. Kaplan, D. L., Boyles, J., Dunlap, B. H., et al. 2014, *Astrophysical Journal*, 789, 119
69. Smedley, S. L., Tout, C. A., Ferrario, L., & Wickramasinghe, D. T. 2014, *Monthly Notices of the Royal Astronomical Society*, 437, 2217
70. Tauris, T. M., & van den Heuvel, E. P. J. 2014, *Astrophysical Journal Letters*, 781, L13
71. Cadelano, M., Pallanca, C., Ferraro, F. R., et al. 2015, *Astrophysical Journal*, 812, 63
72. Jiang, L., Li, X.-D., Dey, J., & Dey, M. 2015, *Astrophysical Journal*, 807, 41
73. Kilic, M., Hermes, J. J., Gianninas, A., & Brown, W. R. 2015, *Monthly Notices of the Royal Astronomical Society*, 446, L26
74. Antoniadis, J., Kaplan, D. L., Stovall, K., et al. 2016, *Astrophysical Journal*, 830, 36
75. Deller, A. T., Vigeland, S. J., Kaplan, D. L., et al. 2016, *Astrophysical Journal*, 828, 8
76. Bassa, C. G., Antoniadis, J., Camilo, F., et al. 2016, *Monthly Notices of the Royal Astronomical Society*, 455, 3806
77. Tremblay, P.-E., Gentile-Fusillo, N., Raddi, R., et al. 2017, *Monthly Notices of the Royal Astronomical Society*, 465, 2849
78. Kleinman, S. J., Kepler, S. O., Koester, D., et al. 2013, *Astrophysical Journals*, 204, 5
79. Kepler, S. O., Pelisoli, I., Koester, D., et al. 2015, *Monthly Notices of the Royal Astronomical Society*, 446, 4078
80. Althaus, L. G., García-Berro, E., Isern, J., & Córscico, A. H. 2005, *Astronomy & Astrophysics*, 441, 689
81. Renedo, I., Althaus, L. G., Miller Bertolami, M. M., et al. 2010, *Astrophysical Journal*, 717, 183
82. Tremblay P.-E., Ludwig H.-G., Steffen M., Freytag B., 2013, *Astronomy & Astrophysics*, 559, A104
83. Koester, D., & Kepler, S. O. 2015, *Astronomy & Astrophysics*, 583, A86
84. Schmidt, M. 1968, *Astrophysical Journal*, 151, 393
85. García-Berro, E., Kilic, M., & Kepler, S. O. 2016, *International Journal of Modern Physics D*, 25, 1630005
86. Kepler S. O., et al., 2013, *Monthly Notices of the Royal Astronomical Society*, 429, 2934
87. Külebi B., Jordan S., Euchner F., Gänsicke B. T., Hirsch H. 2009, *Astronomy & Astrophysics*, 506, 1341
88. Bagnulo, S., & Landstreet, J. D. 2015, *Polarimetry of Stars and Planetary Systems*, 224
89. Bagnulo, S., Fossati, L., Landstreet, J. D., & Izzo, C. 2015, *Astronomy & Astrophysics*, 583, A115
90. Żejmo, M., Słowikowska, A., Krzeszowski, K., Reig, P., & Blinov, D. 2017, *Monthly Notices of the Royal Astronomical Society*, 464, 1294
91. Kholtygin, A. F., Fabrika, S., Hubrig, S., et al. 2017, arXiv:1701.00739
92. Gänsicke B. T., Euchner F., Jordan S., 2002, *Astronomy & Astrophysics*, 394, 957

93. Schmidt G. D., et al., 2003, *Astrophysical Journal*, 595, 1101
94. Clemens J. C., Crain J. A., Anderson R., 2004, SPIE, 5492, 331
95. Brinkworth C. S., Burleigh M. R., Lawrie K., Marsh T. R., Knigge C., 2013, *Astrophysical Journal*, 773, 47
96. Euchner F., Jordan S., Beuermann K., Gänsicke B. T., Hessman F. V., 2002, *Astronomy & Astrophysics*, 390, 633
97. Euchner F., Reinsch K., Jordan S., Beuermann K., Gänsicke B. T., 2005, *Astronomy & Astrophysics*, 442, 651
98. Euchner F., Jordan S., Beuermann K., Reinsch K., Gänsicke B. T., 2006, *Astronomy & Astrophysics*, 451, 671
99. Beuermann K., Euchner F., Reinsch K., Jordan S., Gänsicke B. T., 2007, *Astronomy & Astrophysics*, 463, 647
100. Jordan S., 1992, *Astronomy & Astrophysics*, 265, 570
101. Jordan S., Schmidt H., 2003, ASPC, 288, 625
102. Jordan S., Aznar Cuadrado R., Napiwotzki R., Schmid H. M., Solanki S. K. 2007, *Astronomy & Astrophysics*, 462, 1097
103. Kepler, S. O., Kleinman, S. J., Nitta, A., et al. 2007, *Monthly Notices of the Royal Astronomical Society*, 375, 1315
104. Gianninas A., Bergeron P., Ruiz M. T., 2011, *Astrophysical Journal*, 743, 138
105. Rechenberg, I. 1994, *Werksatt Bionik und Evolutionstechnik* No. 1 (Stuttgart:frommann-holsboog)
106. Friedrich S., Ostreicher R., Ruder H., Zeller G., 1994, *Astronomy & Astrophysics*, 282, 179
107. Muslimov A. G., van Horn H. M., Wood M. A., 1995, *Astrophysical Journal*, 442, 758
108. Ruder H., Wunner G., Herold H., Geyer F., 1994, *Atoms in Strong Magnetic Fields. Quantum Mechanical Treatment and Applications in Astrophysics and Quantum Chaos*, Springer-Verlag, Heidelberg.
109. Schimeczek C., Wunner G., 2014a, *Computer Physics Communications*, 185, 614
110. Schimeczek C., Wunner G., 2014b, *Astrophysical Journals Supplement Series*, 212, 26
111. Schimeczek C., Boblest S., Meyer D., Wunner G., 2013, *Physical Review A*, 88, 012509
112. Valyavin G., et al., 2014, *Nature*, 515, 88
113. Kawaler, S. D. 2015, 19th European Workshop on White Dwarfs, ASPC 493, 65
114. Kawka, A., Vennes, S., Schmidt, G. D., Wickramasinghe, D. T., & Koch, R. 2007, *Astrophysical Journal*, 654, 499
115. Castanheira, B. G., Kepler, S. O., Kleinman, S. J., Nitta, A., & Fraga, L. 2013, *Monthly Notices of the Royal Astronomical Society*, 430, 50
116. Marsh, T. R., Gänsicke, B. T., Hümmelich, S., et al. 2016, *Nature*, 537, 374
117. Beskrovnaya, N. G., & Ikhsanov, N. R. 2016, arXiv:1612.07831
118. Malheiro, M., Rueda, J. A., & Ruffini, R. 2012, *Publication of the Astronomical Society of Japan*, 64, 56
119. Kawka, A., Briggs, G. P., Vennes, S., et al. 2016, arXiv:1612.00325
120. Charpinet, S., Fontaine, G., & Brassard, P. 2009, *Nature*, 461, 501
121. Córscico, A. H., Althaus, L. G., Kawaler, S. D., et al. 2011, *Monthly Notices of the Royal Astronomical Society*, 418, 2519
122. Fontaine, G., Brassard, P., & Charpinet, S. 2013, 18th European White Dwarf Workshop., 469, 115
123. Hermes, J. J., Kawaler, S. D., Bischoff-Kim, A., et al. 2016, arXiv:1612.07807
124. Cantiello, M., Mankovich, C., Bildsten, L., Christensen-Dalsgaard, J., & Paxton, B.

- 2014, *Astrophysical Journal*, 788, 93
125. Fuller, J., Lecoanet, D., Cantiello, M., & Brown, B. 2014, *Astrophysical Journal*, 796, 17
 126. Ringwald, A. 2016, arXiv:1612.08933
 127. Isern, J., & García-Berro, E. 2003, *Nuclear Physics B Proceedings Supplements*, 114, 107
 128. Isern, J., García-Berro, E., Althaus, L. G., & Córscico, A. H. 2010, *Astronomy & Astrophysics*, 512, A86
 129. Córscico, A. H., Althaus, L. G., Miller Bertolami, M. M., et al. 2012, *Monthly Notices of the Royal Astronomical Society*, 424, 2792
 130. Córscico, A. H., Althaus, L. G., Romero, A. D., et al. 2012, *Journal of Cosmology and Astroparticle Physics*, 12, 010
 131. Córscico, A. H., Romero, A. D., Althaus, L. G., et al. 2016, *Journal of Cosmology and Astroparticle Physics*, 7, 036
 132. Battich, T., Córscico, A. H., Althaus, L. G., & Miller Bertolami, M. M. 2016, *Journal of Cosmology and Astroparticle Physics*, 8, 062
 133. Catalán, S., Isern, J., García-Berro, E., & Ribas, I. 2008, *Monthly Notices of the Royal Astronomical Society*, 387, 1693